Improvement of MFL sensing–based damage detection and quantification for steel bar NDE

Ju-Won Kim[1], Minsu Park[2], Junkyeong Kim[2] and Seunghee Park[*1]

[1]School of Civil, Architectural Engineering and Landscape Architecture, Sungkyunkwan University, 2066 Seobu-ro,
Jangan-gu, Suwon 16419, Republic of Korea
[2]Department of Civil & Environmental System Engineering, Sungkyunkwan University, 2066 Seobu-ro,
Jangan-gu, Suwon 16419, Republic of Korea

Abstract. A magnetic flux leakage (MFL) method was applied to detect and quantify defects in a steel bar. A multi-channel MFL sensor head was fabricated using Hall sensors and magnetization yokes with permanent magnets. The MFL sensor head scanned a damaged specimen with five levels of defects to measure the magnetic flux density. A series of signal processing procedures, including an enveloping process based on the Hilbert transform, was performed to clarify the flux leakage signal. The objective damage detection of the enveloped signals was then analyzed by comparing them to a threshold value. To quantitatively analyze the MFL signal according to the damage level, five kinds of damage indices based on the relationship between the enveloped MFL signal and the threshold value were applied. Using the proposed damage indices and the general damage index for the MFL method, the detected MFL signals were quantified and analyzed relative to the magnitude of the damage increase.

Keywords: magnetic flux leakage; steel bar inspection; damage quantification; Hilbert transform; generalized extreme value distribution

1. Introduction

Steel cable is an important member used to fully support loads in structures and transmit power, and it is widely used because of its high strength and flexibility. Steel rods have also been used to connect and fix structures, as well as maintain tension to support a load. Because these members fully support the load on the structure, their health is directly related to the safety of the entire structure.

However, they can be damaged by local defects such as corrosion caused by the external environment, cracking due to unexpected mechanical movement, aging caused by long-term use, and metal loss due to friction. These small defects can expand quickly due to tension on the cable, such that defects in the steel bar or cable can lead to significant accidents, such as structural failure (Abdullah *et al.* 2015).

Some steel rods and cables are used in situ in very dangerous conditions. Such defects are not easily detected due to the characteristics of the steel rods and cables, such as their complex cross-sections and long lengths; defects are often invisible and occur in inaccessible locations (Weischedel 1985).

For these reasons, magnetic sensing based non-destructive evaluation (NDE) methods can be an effective approach for defect detection by taking advantage of the characteristics of the steel members, which are continuous

in a cross section and composed of a ferromagnetic material that is magnetized easily (Shi *et al.* 2015, Wang *et al.* 2005, Weischedel and Chaplin 1991, Yim e*t al.* 2013).

In this study, a magnetic sensing–based NDE method was applied to detect local defects. Among the various magnetic sensing methods (Lenz 1990, Wang *et al.* 2006), the magnetic flux leakage (MFL) method was applied because it is suitable for continuous ferromagnetic members and has been verified in previous studies (Göktepe 2001, Kim *et al.* 2017, Mukhopadhyay and Srivastava 2000, Park *et al.* 2014).

Although many studies have been performed to detect defects using MFL methods, most of these only focused on diagnosing whether defects were present. These studies are therefore limited in that they do not perform measurements that account for the level of damage.

To overcome this limitation, MFL signals were analyzed using damage indices dependent on the damage level in order to quantitatively evaluate the damage (Zhang and Tan 2016). Typically, only two kinds of damage indices have been used to quantify MFL signals for estimating defect size (Boat *et al.* 2014, Li and Zhang 1998, Wilson *et al.* 2008). To improve the accuracy of damage level quantification, damage indices extracted from the relationship between the enveloped MFL signal and the threshold value were additionally applied in this study (Kim and Park 2017).

To verify the feasibility of the proposed MFL method, a series of quantitative experiments was performed. In this study, steel bar specimens on which precise defects could be machined were utilized to represent steel cables and steel

---

∗Corresponding author, Associate Professor
 E-mail: shparkpc@skku.edu

rods. A multi-channel MFL sensor head was also fabricated using Hall sensors and permanent magnets, adapted to the steel bar. The MFL sensor head scanned the specimens, which were formed with artificial damage, to measure the magnetic flux density. The resolution of the measured magnetic flux signal was improved through signal processing. The MFL signals were then analyzed for objective defect detection by comparing them with the threshold value. Finally, the detected MFL signals were quantified according to damage level using various damage indices that depend on the relationship between the enveloped MFL signal and the threshold value.

2. Theoretical background

2.1 MFL-based damage detection method

Magnetized steel materials can be considered magnets. When a small air gap is created by a defect, the magnetic field spreads out because the air cannot support as strong of a magnetic field as the magnetized steel. When the magnetic field leaks out of the material, it is called magnetic flux leakage (Edwards and Palmer 1986).

In order to establish sufficient magnetic flux in the material to be measured, the specimen must be magnetized. In this study, magnetic yokes with strong permanent magnets were used to fully magnetize the steel bar specimens.

The magnetic flux in a specimen is uniform when there is no defect present, as illustrated in Fig. 1(a). In contrast, when there are local defects, magnetic flux leakage occurs around the defect point, as shown in Fig. 1(b).

When the magnetic flux leaks out of a metal specimen near the defects, magnetic sensors placed between the poles of the magnet yoke can be used to detect this leakage.

In this study, Hall sensors, which operate based on the Hall effect, were used to capture the MFL signal, as illustrated in Fig. 2. The sensors generate a voltage signal that is proportional to the magnetic flux leakage (Ramsden, 2006; Lenz, 1990), and these voltage signals are transmitted to the data acquisition (DAQ) system.

(a) intact condition   (b) damaged condition
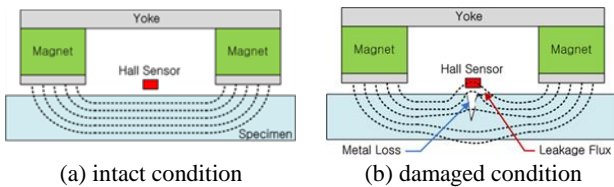
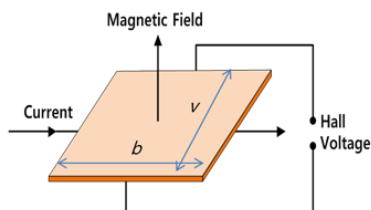Fig. 1 Principle of the MFL method (Park *et al.* 2014)

Fig. 2 Principle of the Hall effect (Coles 2001)

2.2 Signal processing and decision making

Signal processing techniques, such as low-pass filtering and offset correction, were performed to improve the resolution of the signal after measuring the magnetic flux (Kim *et al.* 2015). After the de-noising process, an enveloping process using the Hilbert transform was performed to clarify flux leakage and improve accuracy (Feldman 2006).

To distinguish between the intact and damaged conditions for decision making, a 99.99% confidence level threshold was set for the intact condition using the generalized extreme value (GEV) distribution (Coles 2001), as shown in Fig. 3.

When the enveloped MFL signal exceeds the established threshold value, the signal is determined to represent a damaged condition (Kim e*t al.* 2012).

2.3 Damage indices for quantification

In quantifying the MFL signal, the peak-to-peak value (P-Pv), shown in Fig. 4(a), has typically been used to represent the y-component of the leakage field, which relates to the depth of damage. The x-component of the leakage field is represented by the peak-to-peak width (P-Pw), as shown in Fig. 4(b) (Li and Zhang 1998, Xu *et al.* 1996).

In this study, three new types of damage indices are applied to quantify the damage level. These indices are extracted from the relationship between the enveloped signal after signal processing and the threshold value.

The maximum peak of the enveloped signal that exceeds the threshold was extracted, as shown in Fig. 4(c), and is referred to as the 'peak value of the envelope (E_P).' Also, a damage index called the 'width of the envelope (E_W)' was determined by calculating the range over which the envelope exceeds the threshold value, as shown in Fig. 4(d); this represents the x-component of the leakage field. In addition, to account for the shape of the envelope signal, the area of the envelope (E_A) was extracted by integrating the amplitude of the signal in the threshold-exceeding range, as shown in Fig. 4(e). Thus, even if the height and width are the same, the area of the envelope can reflect the shape of the enveloped MFL signal.
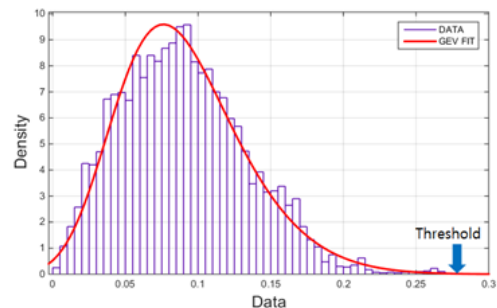

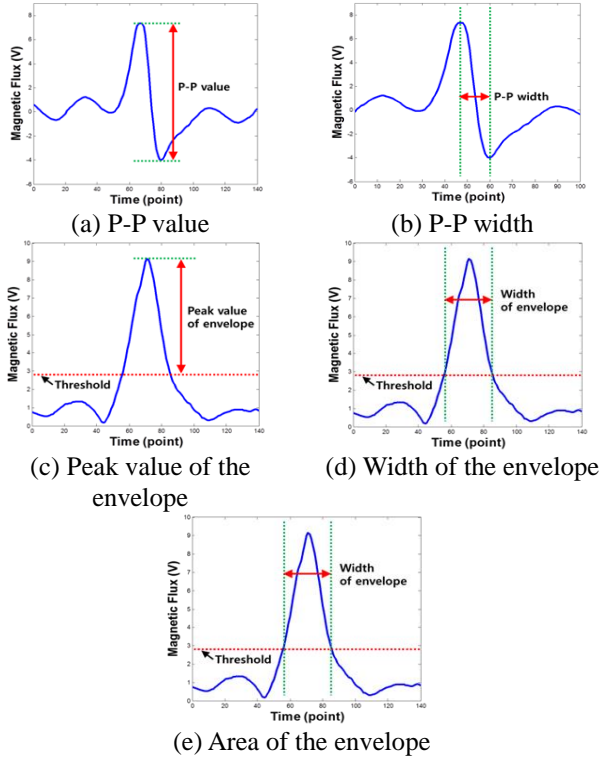Fig. 3 Threshold established using the GEV distribution

(a) P-P value

(b) P-P width

(c) Peak value of the envelope

(d) Width of the envelope

(e) Area of the envelope

Fig. 4 Damage indices for quantifying the MFL signal

3. Multi-channel MFL sensor head fabrication

To verify the proposed NDE method experimentally, a multi-channel MFL sensor head was fabricated to measure the magnetic flux signals from the steel bar specimen.

In this study, the sensor head was composed of eight channels on the sensor module, which were circumferentially arranged in a circular configuration in order to obtain signals from the entire cross-section of the specimen (Lee *et al.* 2009, Sharatchandra *et al.* 2012), as shown in Fig. 5.

Each sensor module was composed of a magnetization component that created a magnetic field for magnetizing the specimen and a sensing component to measure the magnetic flux signal, as shown in Fig. 6.

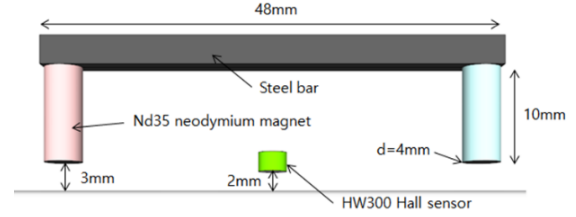Fig. 5 Design of the multi-channel MFL sensor head and configuration of the sensing channels

Fig. 6 Specifications of the sensor module

The magnetization component was a permanent magnetic yoke consisting of two high-strength Nd-Fe-B magnets (neodymium 35) and a steel bar. The advantage of the permanent magnets is that no power is required for operation, enabling a lighter system than that required to use an electromagnet.

The sensing component was composed of a Hall sensor (HW300) located at the center of the magnetization yoke. Each Hall sensor converts the magnetic flux signal to a voltage signal that is transmitted to the DAQ system.

A magnetization yoke and a Hall sensor were assembled along with wheels using an aluminum frame to make a sensor module, as shown in Fig. 7.

Then, eight sensor modules were connected using elastic rubber O-rings to maintain a constant lift-off which is very important for constant sensitivity (Yang *et al.* 2008). This joining method also helped protect the sensor head by preventing the impact from changes in the diameter of the specimen due to the flexible expansion and contraction motion of independent sensor modules.
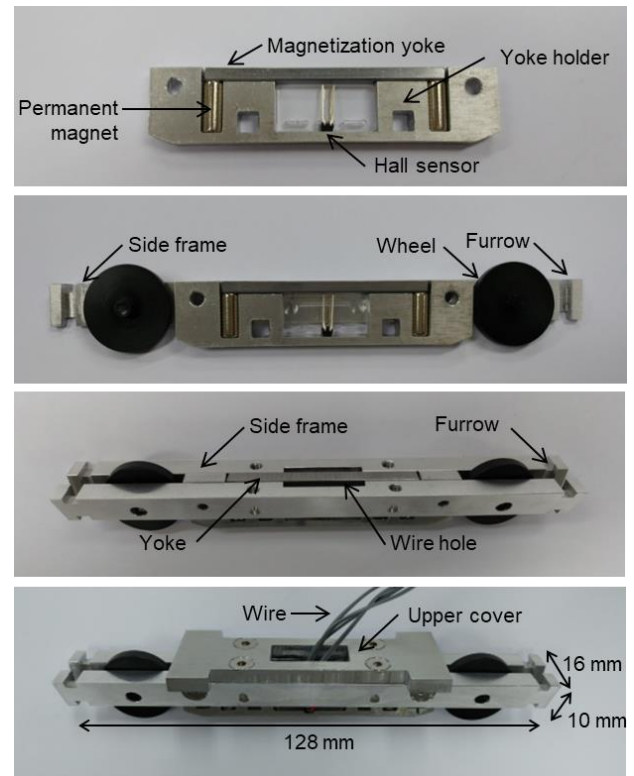

Fig. 7 Fabrication of the MFL sensor module

4. Experimental study

4.1 Experimental setup and procedure

A series of experimental studies were performed to examine the capabilities of the damage detection technique.

Steel bar specimens 10 mm in diameter and 800 mm in length were prepared, and artificial defects of several sizes were formed on the specimens.

The test setup for MFL-based damage detection was composed of the MFL sensor head, a compact DAQ, and a terminal board, as shown in Figs. 8 and 9.

The sensor head had eight sensing channels for data acquisition, where each channel consisted of a Hall sensor, a carbon steel yoke, and two permanent magnets with different polarizations. The linear motion equipment caused the MFL sensor head to move linearly on the steel bar specimen at a constant velocity of 1 m/s.

The data acquisition equipment, which consisted of a terminal board and a compact DAQ, measured the MFL voltage from the specimen using Hall sensors at the MFL sensor head.

The magnetic flux signal was measured 25 times at each damage level. The measured signals were then processed using a signal processing and enveloping process based on the Hilbert transform in order to facilitate effective damage detection.
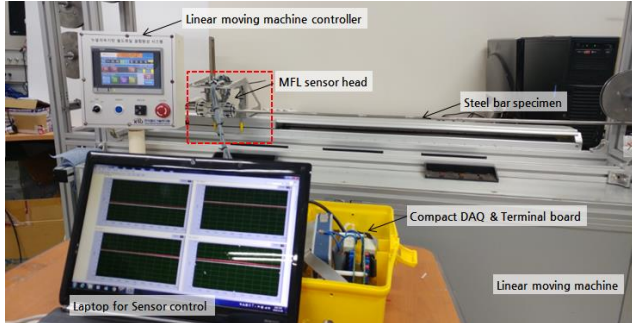

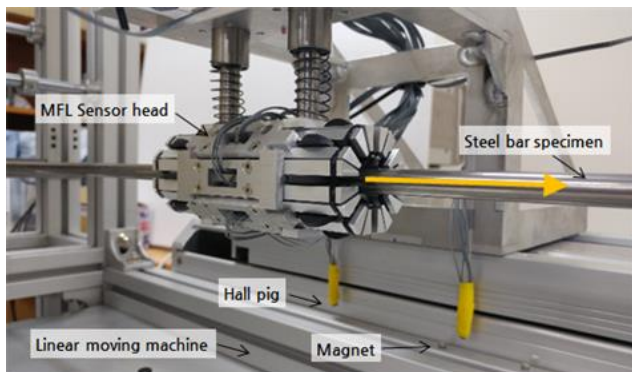Fig. 8 Test setup for magnetic flux signal measurement

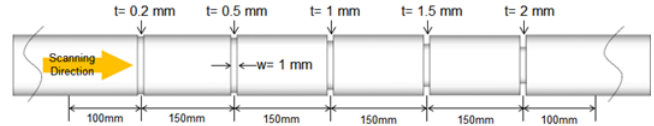Fig. 9 Sensor head for scanning the steel bar specimen

Fig. 10 Steel bar specimen for the defect depth test

4.2 MFL signal as a function of depth

4.2.1 Experimental procedure and specimen

To analyze the characteristics of the MFL signal as a function of defect depth, a steel bar specimen 10 mm in diameter and 800 mm in length was prepared, and five levels of artificial defects with different depths from 0.2 mm to 2 mm were formed on the specimen, as shown in Fig. 10.

Before the experiment, the eight-channel sensor head was calibrated for sensitivity using an empirical method (Mukherjee *et al.* 2012). Magnetic flux signals were then measured from the eight sensor channels simultaneously.

4.2.2 Experimental results for depth increase

The enveloped signals after signal processing were averaged over the 25 measurements from each channel and are displayed in Fig. 11.

As shown in Figure 11, an enveloped MFL signal was detected at 100 mm, 250 mm, 400 mm, 550 mm, and 700 mm in all sensing channels. These locations corresponded with the real locations of the defects. This means that MFL signals could be effectively obtained at the actual damage point using this MFL-based NDE method.

The enveloped magnetic flux signals collected from the eight sensing channels were overlapped and are shown in Fig. 12 along with the threshold line, which was established to be 0.78 V and is indicated by a red dotted line.
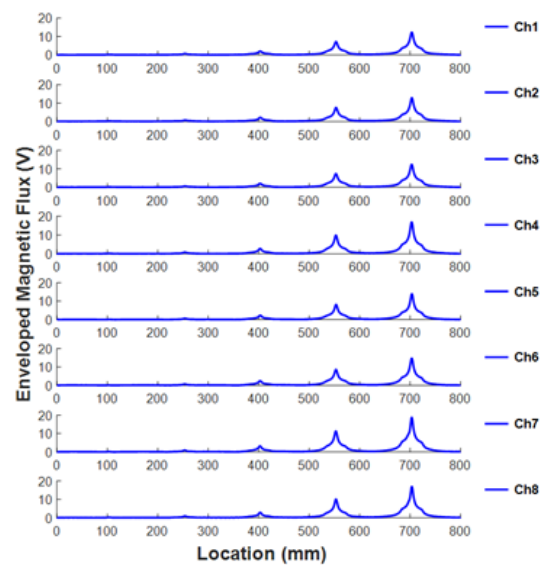

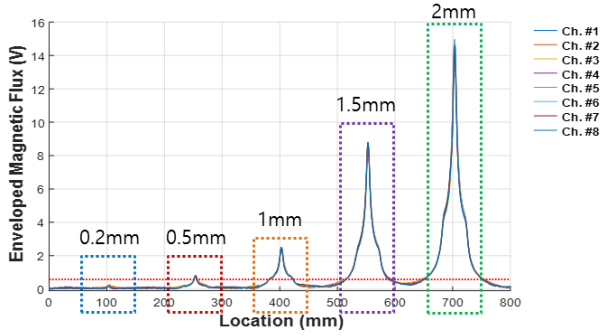Fig. 11 Enveloped signals with depth increase

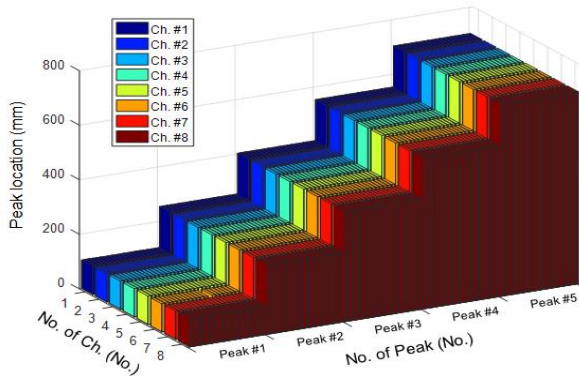Fig. 12 Overlapped enveloped signals for the defect depth test

Fig. 13 Estimated damage location in each channel for the defect depth test

(a) MFL signal

(b) Enveloped signal

Fig. 14 MFL signals as a function of defect depth

Fig. 15 P-P value for the defect depth test

As shown in Fig. 12, at all damage levels except 0.2 mm, the enveloped signals exceeded the threshold, with these signals occurring at 250 mm, 400 mm, 550 mm, and 700 mm in all sensing channels. This means that defects with a depth exceeding 0.5 mm can be detected by comparing the enveloped MFL signal and the threshold value.
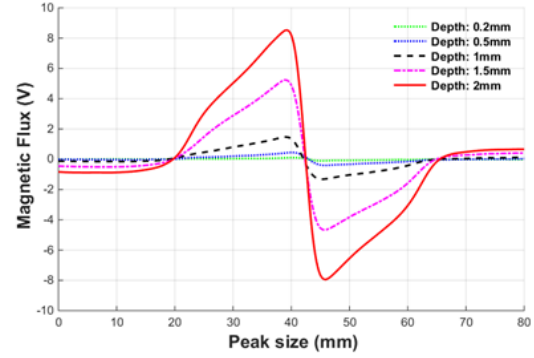
Fig. 13 shows the estimated location of the defect extracted from the repeatedly measured MFL signals.

At all channels and all measurement times, constant locations within a maximum deviation of 0.74 mm were estimated, all of which were the same as the actual locations of the damage.
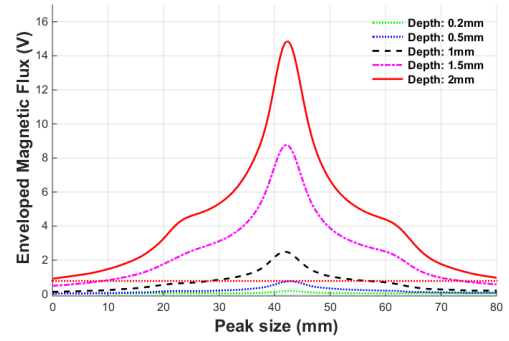
To compare the MFL signals to each other according to depth, the MFL signal and the enveloped signal from each depth level were overlapped, as shown in Fig. 14.

The size of the flux leakage signals from the defects increased as the depth of the defects increased, as shown in Fig. 14(a). Fig. 14(b) shows that the height and width of the enveloped signal increased as the depth of damage increased. This implies a proportional relationship between the depth of damage and the size of the MFL signal.

Damage indices were extracted using an automated damage extraction algorithm to quantify the extent of the damages. Each extracted damage index is displayed as the mean value and the maximum error value.
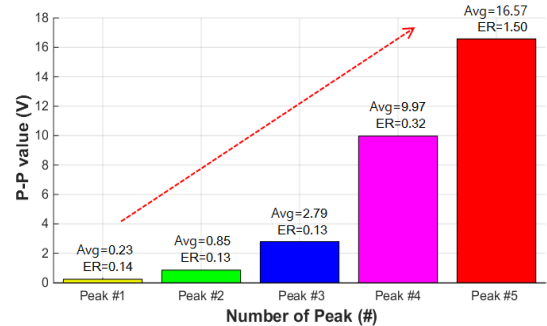
The P-P value and P-P width that are commonly utilized to analyze MFL signals were calculated using the raw MFL signals. Figs. 15 and 16 show graphs of the P-P value and P-P width extracted from the raw signals in the depth increase test.

As known for the MFL method, the P-P value effectively quantified the depth of damage, increasing gradationally as the depth increased, as shown in Fig. 15.

In contrast, although errors existed at a depth of 0.2 mm, the P-P width values were constant regardless of the depth, as shown in Fig. 16.

To improve quantification accuracy, the peak value of the envelope (E_P) and the width of the envelope (E_W) were also found using the relationship between the enveloped signals and the threshold value. Figs. 17 and 18 show graphs of the peak value of the envelope and the width of the envelope as a function of the depth of damage.
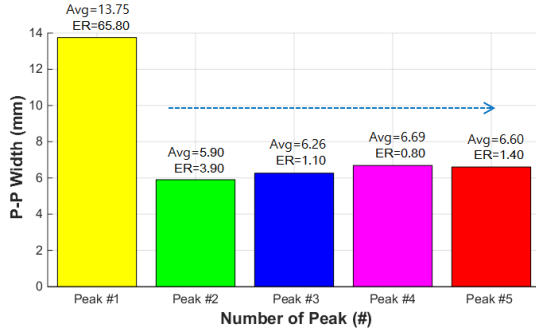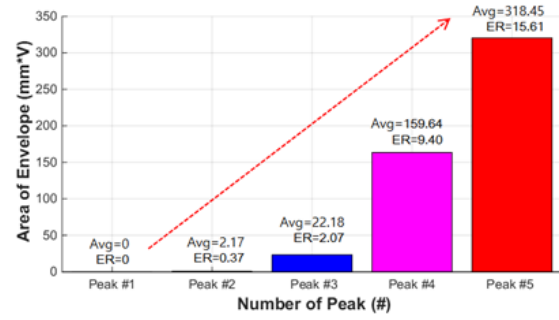
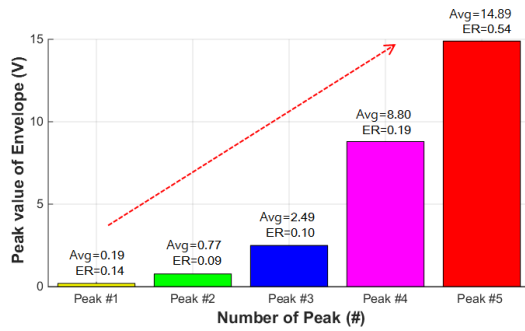Fig. 16 P-P width for the defect depth test

Fig. 17 Peak value of the envelope for the defect depth test
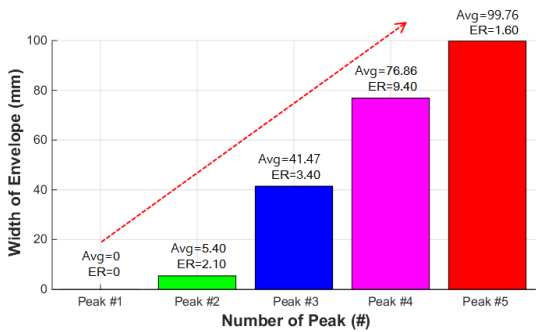

Fig. 18 Width of the envelope for the defect depth test

The peak value of the envelope increased stepwise with the increase in the depth of damage, similar to the P-P value.

However, the width of the envelope (E_W) also increased with the depth increase, unlike the P-P width.

Next, the area of the envelope, reflecting both the height and width of the peak, was extracted and is shown in Fig. 19.

As expected based on the peak value of the envelope and the width of the envelope, the area of the envelope rapidly increased as the depth of the defect increased.

Therefore, it was demonstrated that all of the proposed damage indices, except the P-P width, were positively correlated with the depth of the defect. Therefore, they are considered to be effective indices for quantifying the depth of damage.

Fig. 19 Area of the envelope for the defect depth test

4.3 MFL signal as a function of width

4.3.1 Experimental procedure and specimen

To analyze the characteristics of the MFL signal as a function of the width of the damage, a steel bar specimen 10 mm in diameter and 800 mm in length was fabricated with five defects of stepwise increasing width, as shown in Fig. 20.

As shown in Fig. 20, the depths of the defects were all the same, and widths were 0.5 mm, 1 mm, 3 mm, 6 mm, and 9 mm. These defects were located at 100 mm, 250 mm, 400 mm, 550 mm, and 700 mm, respectively. The magnetic flux signals were measured 25 times at a velocity of 1 m/s.

4.3.2 Experimental results of the width test

Fig. 21 shows the enveloped signals obtained from each channel after removing the noise.

As shown in Fig. 21, MFL signals were detected at 100 mm, 250 mm, 400 mm, 550 mm, and 700 mm in each sensing channel, corresponding to the locations of the actual damage.

In addition, the envelope signal exceeded the threshold value indicated by the red dotted line, again established as 0.78 V, at all five damage points. Therefore, all were therefore determined to be damaged.

Fig. 22 shows the estimated location of the defect centers extracted from the repeatedly measured MFL signals.

At all channels and all measurement times, constant locations were estimated, all of which were the same as the actual locations of the damage.

The signals for each channel are superimposed in Fig. 23. The maximum deviation of the peaks measured in each channel was within 0.2 V, indicating that there was almost no sensitivity difference between the channels.
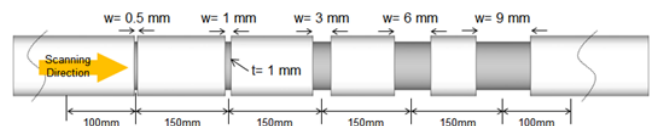

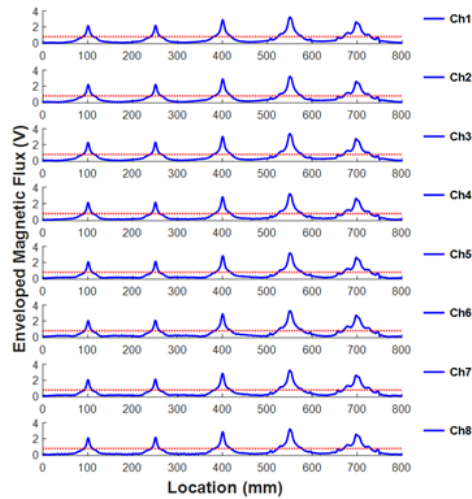Fig. 20 Steel bar specimen for the defect width test

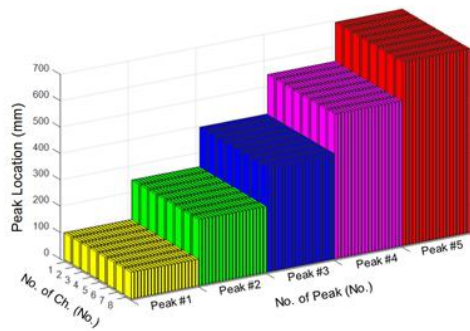Fig. 21 Enveloped signals for the defect width test

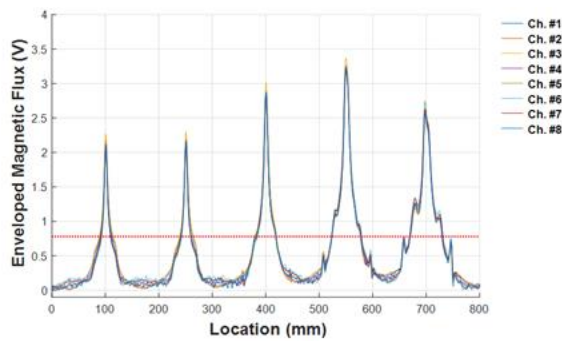Fig. 22 Estimated damage location in each channel for the defect width test

Fig. 23 Overlapped enveloped signals for the width test

To analyze the variation in the MFL signal due to the increase in the damage width, each peak corresponding to a damage point was plotted and overlapped, as shown in Fig. 24. In this plot, the mean value of the 25 measured MFL signals was used.

Fig. 24 shows that the width of the MFL signal increased as the width of the damage increased from 1 mm (defects #1 and #2) to 9 mm (defect #5). From this, it follows that the peak-to-peak distance increases as the width of the damage increases.
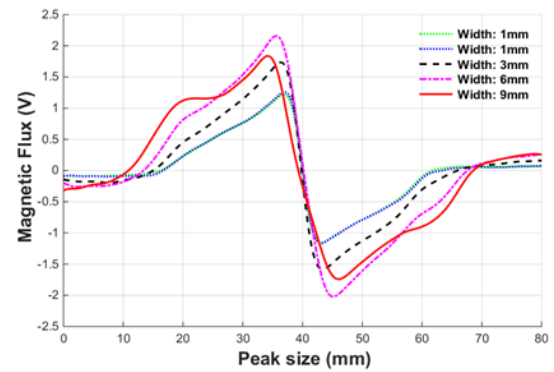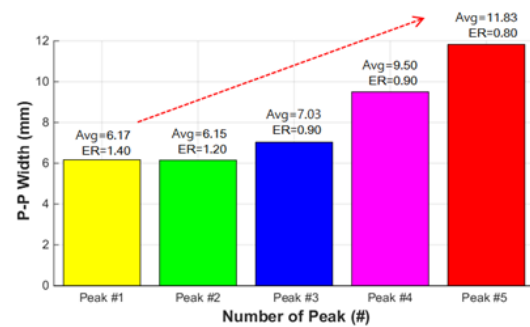

Fig. 24 MFL signals according to defect width

Fig. 25 P-P width for the defect width test

The P-P width, which is a damage index that indicates the distance between peaks, was extracted for each measurement time and channel and is displayed in Fig. 25.

Based on the results of P-P width extraction shown in Fig. 25, the P-P width is effective for quantifying the width of the damage; although measurement errors existed, the P-P width gradually increased as the width of damage increased.

The mean enveloped magnetic flux signals at each width were overlapped and plotted with the threshold line in Fig. 26.
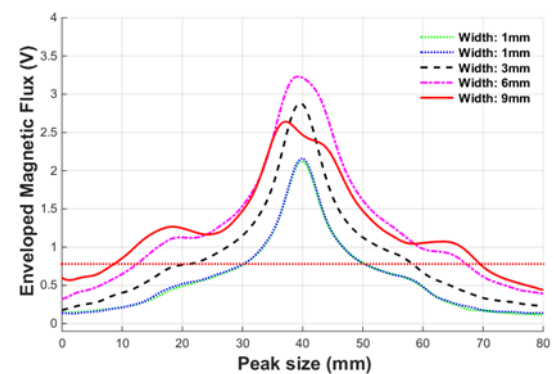

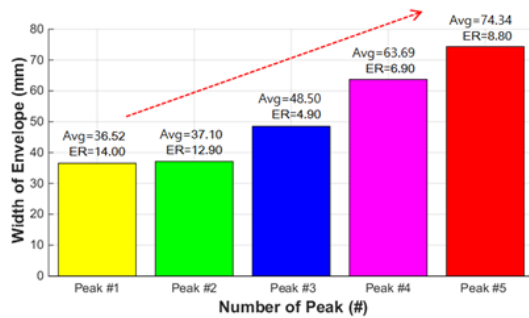Fig. 26 Enveloped MFL signals according to defect width

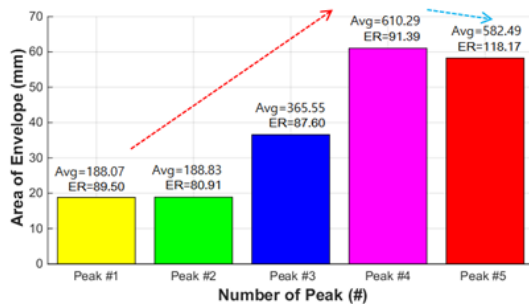Fig. 27 Width of the envelope for the defect width test

Fig. 28 Area of the envelope for the defect width test

As shown in Fig. 26, the peak amplitude increased as the width increased from 1 to 6 mm, but decreased when the width increased to 9 mm.

In contrast, the width of the envelope increased as the width of the damage increased.

The upper part of the peak was narrower at a width of 9 mm than at a width of 6 mm due to the distorted shape of the peak.

However, the width of the envelope at the threshold line (0.78 V), where the width of the envelope index was extracted, gradually increased with the width of the damage.

The width of the envelope, which represents the width of the envelope exceeding the threshold, was extracted and is shown in Fig. 27.

Although error existed between the measurements, the difference in the width of the envelope for each damage width increase was greater than the error. Therefore, this damage index clearly classified the defects without misrecognition due to the influence of the error, and it gradually increased as the defect width increased.

Next, the area of the envelope was extracted and is shown in Fig. 28.

The area of the envelope increased up to a defect width of 6 mm, but was smaller at 9 mm than at 6 mm.

The reason for this is likely because the decrease in amplitude due to the distortion of the peaks was reflected more in the area than the width, even though the width of the envelope increased.

Through this experiment, which used steel bar specimens to analyze the characteristics of the MFL signal as a function of the width of the damage, it was confirmed that the P-P width and the width of the envelope had a positive correlation with the defect width and therefore can

be used as reliable indices for estimating the width of the damage.

5. Conclusions

An MFL sensing–based NDE method was proposed to detect damage in a steel bar. A multi-channel MFL sensor head was fabricated, and a series of experimental studies was performed to verify the feasibility of the proposed technique. In addition, damage indices were extracted to quantify the MFL signal according to damage level and were confirmed to be valid via the following observations:

- MFL signals were detected at the locations of actual damages using the MFL sensor head.
- The envelope of the MFL signal exceeded the threshold determined by the GEV distribution at the actual damage area.
- Damage indices based on the relationship between the envelope signal and the threshold were extracted to quantify the MFL signals; these damage indices could quantify the damage level according to the size of the damage.
- The characteristics of the MFL signal with increasing depth of damage were analyzed, and both the amplitude and width of the peak increased as the depth of damage increased.
- By quantifying the MFL signal according to the defect depth, the damage indices the peak value of the envelope. The P-P value, and width of the envelope were determined to be useful, and all showed a positive correlation with defect depth.
- The width of the peak was shown to increase with defect width. When the MFL signal was quantified using damage indices, the P-P width and width of the envelope were determined to be useful for determining the width of the damage.

References

Abdullah, A.B.M., Rice, J.A. and Hamilton, H.R. (2015), "A strain-based wire breakage identification algorithm for unbonded PT tendons", *Smart Struct. Syst.*, **16**(3), 415-433.

Boat, M., Pearson, N. and Lieb, R. (2014), "The factors that affect the defect sizing capabilities of the Magnetic Flux Leakage Technique", *Proceedings of the 53rd Annual Conference of the*

British Institute of Non-Destructive Testing, Manchester, September.

Coles, S. (2001), *An Introduction to Statistical Modeling of Extreme Values,* Springer, Berlin, Germany.

Edwards, C. and Palmer, S.B. (1986), "The magnetic leakage field of surface-breaking cracks", *J. Phys. D. Appl. Phys.*, **19**(4), 657-673.

Feldman, M. (2006), "Time-varying decomposition and analysis based on the Hilbert transform", *J. Sound. Vib.*, **295**(3-5), 518-530.

Göktepe, M. (2001), "Non-destructive crack detection by capturing local flux leakage field", *Sens. Actuat. A Phys.*, **91**(1-2), 70-72.

Kim, J., Kim, J.W., Lee, C. and Park, S. (2017), "Development of embedded EM sensors for estimating tensile forces of PSC girder bridges", *Sensors*, **17**, E1989.

Kim, J.W. and Park. S. (2017), "Magnetic flux leakage–based local damage detection and quantification for steel wire rope non-destructive evaluation", *J. Intel. Mat. Syst. Str.*, In press.

Kim, J.W., Kim, J., Park. S. and Oh, T. (2014), "Integrating embedded piezoelectric sensors with continuous wavelet transforms for real-time concrete curing strength monitoring", *Struct. Infrastruct. E.* **11**(7), 897-903.

Kim, J.W., Lee, C. and Park. S. (2012), "Damage localization for CFRP-debonding defects using piezoelectric SHM techniques", *Res. Nondestruct. Eval.*, **23**(4), 183-196.

Lee, J., Hwang, J., Jun, J. and Choi, S. (2008), "Nondestructive testing and crack evaluation of ferromagnetic material by using the linearly integrated hall sensor array", *J. Mech. Sci. Technol.*, **22**, 2310-2317.

Lenz, J.E. (1990), "A review of magnetic sensors", *Proc. of the IEEE,* **78**(6), 973-989.

Li, L.M. and Zhang, J.J. (1998), *Characterizing the Surface Crack Size by Magnetic Flux Leakage Testing, In: Nondestructive Characterization of Materials VIII,* Springer, Boston, USA.

Mukherjee, D., Saha, S. and Mukhopadhyay, S. (2012), "An adaptive channel equalization algorithm for MFL signal", *NDT & E Int.,* **45**(1), 111-119.

Mukhopadhyay, S. and Srivastava, G.P. (2000), "Characterisation of metal loss defects from magnetic flux leakage signals with discrete wavelet transform", *NDT&E Int.*, **33**(1), 57-65.

Park, S., Kim, J.W., Lee, C. and Lee, J.J. (2014), "Magnetic flux leakage sensing-based steel cable NDE technique", *J. Shock. Vib.*, **2014**, E929341.

Ramsden, E. (2006), *Hall-effect Sensors: Theory and Applications.* 2nd Ed., Newnes Books, Oxford, UK.

Sharatchandra, W.S., Rao, B.P.C., Thirunavukkarasu, S. and Jayakumar, T. (2012), "Flexible GMR sensor array for magnetic flux leakage testing of steel track ropes", *J. Sensors*, **2012**, E129074.

Shi, Y., Zhang, C., Li, R., Cai, M. and Jia, G. (2015), "Theory and application of magnetic flux leakage pipeline detection", *Sensors*, **15**(12), 31036-31055.

Wang, G., Wang, M.L., Zhao, Y., Chen, Y. and Sun, B. (2006), "Application of magnetoelastic stress sensors in large steel cables", *Smart Struct. Syst.*, **2**(2), 155-169.

Wang, M.L., Wang, G. and Zhao, Y. (2005), *Sensing Issues in Civil Structural Health Monitoring*, Springer, Dordrecht, Netherlands.

Weischedel, H.R. (1985), "The inspection of wire ropes in service: a critical review", *Mater. Eval.*, **43**(13), 1592-1605.

Weischedel, H.R. and Chaplin, C.R. (1991), "Inspection of wire ropes for offshore applications", *Mater. Eval.*, **49**(3), 362-367.

Wilson, J.W., Kaba, M. and Tian, G.Y. (2008), "New techniques for the quantification of defects through pulsed magnetic flux leakage", *Proceedings of the 17th World Conference on Non-destructive Testing*, Shanghai, China, October.

Xue, H., Yang, K. and Yang, S. (1996), "Quantitative inspection of broken wire in wire ropes: method and apparatus", *Int. J. Occup. Saf. Ergo.*, **2**(1), 35-40.

Yang, L., Zhang, G., Liu, G. and Gao, S. (2008) "Effect of lift-off on pipeline magnetic flux leakage inspection", *Proceedings of the 17th World Conference on Nondestructive Testing*, Shanghai, China, October.

Yim, J., Wang, M.L., Shin, S.W., Yun, C.B., Jung, H.J., Kim, J.T. and Eem, S.H. (2013), "Field application of elasto-magnetic stress sensors for monitoring of cable tension force in cable-stayed bridges", *Smart Struct. Syst.*, **12**(3), 465-482.

Zhang, J. and Tan, X. (2016), "Quantitative inspection of remanence of broken wire rope based on compressed sensing", *Sensors*, **16**(9), E1366.